Applied Catalysis B: Environmental 251 (2019) 130–142

Contents lists available at ScienceDirect

Applied Catalysis B: Environmental

journal homepage: www.elsevier.com/locate/apcatb

Visible light assisted thermocatalytic reaction of CO + NO over $Pd/LaFeO_3$

Gang Cheng[a,b], Xiaofang Tan[a,b], Xinjie Song[a,b], Xun Chen[a], Wenxin Dai[a,b,*], Rusheng Yuan[a,**], Xianzhi Fu[a]

[a] Research Institute of Photocatalysis, State Key Laboratory of Photocatalysis on Energy and Environment, Fuzhou University, Fuzhou 350002, China
[b] Key Laboratory of Eco-materials Advanced Technology (Fuzhou University), Fujian Province University, Fuzhou 350002, China

ARTICLE INFO

Keywords:
NO reduction
Carbon monoxide
$Pd/LaFeO_3$
Electron transfer
Photo-assisted effect

ABSTRACT

A $LaFeO_3$ supported Pd nanoparticle catalyst $Pd/LaFeO_3$ was prepared by a two-step precipitation–deposition method. Its catalytic performance for the reduction of NO by CO was subsequently evaluated in the lower temperature under visible light irradiation or not. It was found that visible light could boost the progress of the reaction and the selectivity of forming N_2. The results of temperature-programmed desorption (TPD) of CO and *in-situ* diffuse reflectance infrared Fourier transform spectra (*in-situ* DRIFTS) showed that visible light could enhance the adsorption of NO and its activation at Pd or $LaFeO_3$ site and that of CO at Pd site, respectively. Co-adsorption results of NO + CO suggested that the activated intermediates of CO and NO would further interact to form the isocyanate (–NCO) and N_2O species, which finally transformed to N_2 and CO_2. Based on the results of Raman spectrum, H_2-temperature programmed reduction (TPR), the X-ray photoelectron spectroscopy (XPS), photoluminescence spectra (PL) and photocurrent testing, it was proposed that visible light irradiation could cause the increase in surface electron density of Pd nanoparticles by the photo-induced electron (from O_{2p} to Fe_{3d} orbit) transfer from $LaFeO_3$ to Pd. Moreover, the valence exchange of Fe^{4+} and Fe^{3+} induced by visible light could promote the formation of oxygen vacancies and then the adsorption and activation of CO and NO. This result also indicated that the photo-excitation of supports could strengthen the strong interaction between support and metal nanoparticles, and then promote the thermo-catalytic reactivity of catalysts.

1. Introduction

The rapid growth in the number of automobiles produces a great deal of exhaust gas, especially the NO, CO and HCs [1]. In the past decades, thermo-catalytic reduction of NO with CO as one of the significant three-way conversion reactions (TWC reactions) focusing mostly on utilizing noble metals [2,3], such as Pt, Rh, Pd supported on the metal oxides or perovskite-type oxides [4,5] has been extensively studied and applied at high temperature.

For the reduction of NO by CO in the thermo-catalytic model reaction, it is widely reported that the adsorption and dissociation of NO are the key steps while the surface oxygen vacancy (SOV) can effectively activate the N–O bond then promote its dissociation [6–8]. Similarly, Linsebigler et al. [9] and Dai et al. [10] also reported that oxygen vacancy could positively promote the adsorption and oxidation of CO. Furthermore, El-Bahy [11] has ever investigated the interactions on Pt and Ce-containing catalysts supported on TiO_2, suggesting that the strong interaction between CeO_2 and TiO_2 could facilitate the adsorption of CO, NO and their activation at Pt sites, accompanied with the formation of the –NCO intermediate species. Yao et al. [6] also reported that a Sn doped CeO_2 based catalyst could cause the increase in surface synergetic oxygen vacancies and the surface active sites, which facilitated the adsorption and activation of CO species at the oxygen vacancies. These results all indicated that the CO + NO redox reaction would be mainly dominated by the adsorption and activation of CO and NO at catalyst surface. Additionally, Our previous works [12–14] had reported that introducing light into the thermo-catalytic reaction system of CO oxidation over Au/TiO_2, CO_2 methanation over $Ru/N–TiO_2$ or CO methanation over Ni/TiO_2 catalysts could promote the adsorption of CO or CO_2 and their activation on respective catalyst surface due to the enrichment in surface electron density of Au, Ru or Ni nanoparticles (the photo-generated electrons from TiO_2 induced by light irradiation to the adjacent metallic nanoparticles). Obviously, the photo-assisted effects of catalysts could reduce the reaction temperature and enhance catalytic performance. Based on the above viewpoint, we further introduced UV light irradiation into the CO + NO thermo-

* Corresponding author at: Research Institute of Photocatalysis, State Key Laboratory of Photocatalysis on Energy and Environment, Fuzhou University, Fuzhou 350002, China.
** Corresponding author.
E-mail addresses: daiwenxin@fzu.edu.cn (W. Dai), yuanrs@fzu.edu.cn (R. Yuan).

https://doi.org/10.1016/j.apcatb.2019.03.029
Received 30 October 2018; Received in revised form 29 January 2019; Accepted 12 March 2019
Available online 18 March 2019
0926-3373/

catalytic reduction systems over Pt/TiO_2 or Pt/CeO_2–TiO_2 catalysts [15]. It was found that the photo-assisted catalytic effect actually occurred on this reaction system, which could be also attributed to the intensive adsorption and activation for CO and NO molecules induced by the rich electron density of Pt nanoparticles. This study indicates that the promoted effects stemming from the interaction between the photo-response support and active metal sites maybe also occur on the CO + NO redox reaction over other catalysts.

Since $LaFeO_3$ [16–18], as a La-based perovskites oxide with a general formula ABO_3, possesses the excellent thermal stability, non-toxicity, outstanding redox properties, alternative A or B site constituting elements, especially the high oxygen vacancy concentration and reversible migration ability of lattice oxygen due to the co-existence of mixture valence at active B site of perovskites, it was also investigated and considered as alternative TWC catalysts or supports to partially substitute for the traditional noble metal based TWC, such as the Pd doped or impregnated perovskite oxides [4,5,19,20]. Besides, it has been ever reported that the perovskite based oxides could be full of capacities as support material for stabilizing the dispersion of noble metals and then enhancing their catalytic performances for high-temperature catalytic applications [4,21]. Moreover, as a semiconductor, $LaFeO_3$ was widely applied in the photocatalytic decomposition of water, degradation of dyes and oxidation of organic pollutants under visible light irradiation due to its suitable band gap of 2.1 eV, which can adequately utilize visible light [18,22,23]. In addition, as one of the widely co-catalysts, Pd was frequently employed as an active species to activate CO and NO adsorbed on its surface in the thermocatalytic reaction [3,24]. Valden et al. [25] have ever focused on examining the adsorption and decomposition of CO and NO on Pd catalysts and proposed that different chemical states of Pd site in supports would affect the CO and NO adsorption significantly. Ozensoy et al. [26] also investigated the CO + NO reaction on the various Pd model catalysts by an *in-situ* infrared vibrational spectroscopy testing, and found that the CO or NO adsorption on the surface of Pd (111) would be activated to form a crucial reaction intermediate, isocyanate (–NCO). Moreover, Ueda et al. [27] also reported that the supported Pd nanoparticles were more efficient than that of the supported Pt nanoparticles in the selectivity of N_2, especially deposited on the reducible supports, such as TiO_2. Based on the above properties of $LaFeO_3$ and Pd, we think that a $LaFeO_3$ supported Pd catalyst ($Pd/LaFeO_3$) maybe own a better catalytic performance for CO + NO redox reaction at a low temperature under visible light irradiation.

Therefore, in this work we have prepared a series of $Pd/LaFeO_3$ catalysts by a two-step precipitation–deposition method, and investigated the behaviors of visible light on the thermo-catalytic reaction of CO + NO over $Pd/LaFeO_3$ at a lower temperature. It was expected that the visible light irradiation could further promote the activation of CO or NO species adsorbed at catalyst surface, and then enhance the catalytic activity. Fortunately, the results demonstrated that visible light actually facilitated the catalytic activities of $Pd/LaFeO_3$ for CO + NO reaction. After UV–vis diffuse reflectance spectroscopy (DRS), temperature-programmed desorption (TPD), the X-ray photoelectron spectroscopy (XPS) testing and *in-situ* diffuse reflectance infrared Fourier transform spectra (*in-situ* DRIFTS) techniques, a possible reaction mechanism for the photo-assisted NO reduction by CO over the $Pd/LaFeO_3$ was proposed as well.

2. Experimental

2.1. Catalyst preparation

The $LaFeO_3$ powder was prepared by a facile co-precipitation method [19]. Firstly, a 1.8 g polyvinylpyrrolidone (PVP, M_{av} = 40,000) was absolutely dissolved in 40 mL isopropanol at room temperature, then a 1.5 mL HNO_3, 5 mmol $Fe(NO_3)_3{\cdot}9H_2O$ and 5 mmol $La(NO_3)_3{\cdot}6H_2O$ were added into the transparent solution in order. This obtained viscous solution was vigorously stirred for 12 h and then was oven dried at 80 °C for 48 h. Finally, the resulted yellow power was ground and calcined at 400 °C in air for 4 h at a ramping rate of 1 °C min^{-1} followed by calcining at 600 °C in air for 2 h with a ramping rate of 5 °C min^{-1}.

The $LaFeO_3$ supported Pd sample ($Pd/LaFeO_3$) was prepared by a deposition precipitation method. A 1.2 g $LaFeO_3$ powder first was first scattered in a beaker with 100 mL deionized water. Then 10 mL $PdCl_2$ (1.2 mg mL^{-1}) was added into the above solution. After stirring it for 2 h, the pH value was adjusted to 10 with 0.1 M NaOH solution. An excessive $NaBH_4$ aqueous solution (0.1 M) was added into the mixture for reducing the Pd ions into the metallic Pd. After keeping stirring for another 2 h, the precipitation was washed and filtered repeatedly with deionized water until the Na^+ and Cl^- were removed. Finally, the obtained $Pd/LaFeO_3$ (the loading amount of Pd was about 1.0 wt%) was dried in vacuum oven at 60 °C overnight.

2.2. Characterization of catalysts

The X-ray diffraction patterns (XRD) patterns were recorded on a Bruker D8 advance powder X-ray diffractometer using Cu Kα irradiation (λ = 0.15418 nm) operated at 40 kV and 40 mA. The mean crystallite size was determined by the strongest peak of the sample with the Debye–Scherrer-equation $d = K\lambda/b\cos\theta$. Raman spectra were collected on LabRAM HR UV-NIR microscope (HoRIBA Jobin Yvon) employing a 532 nm excition of Ar^+ ion laser. The Brunauer–Emmett–Teller (BET) specific surface area and the pore size distribution curves of samples were determined using a Micromeritics ASAP 2020 surface area analyser with nitrogen adsorption at 77 K. The morphologies and the structures of the catalysts were taken on a SU8010 (Hitachi) field emission scanning electron microscope (SEM) and transmission electron microscopy (TEM) investigation (JEOL JEM-2010EX with field emission gun at 200 kV). The compositions of the samples were analyzed by energy-dispersive X-ray spectroscope (EDX) attached to the TEM instrument. The DRS were recorded at room temperature by a UV–vis spectrophotometer (Agilent, Cary 5000) equipped with an integrating sphere and BaSO4 was employed as a reference. The XPS measurements were performed on a Thermo Fisher Scientific ESCALAB 250Xi spectrometer system by using the Al-Kα X-ray beam (1486.6 eV) with the C1s (284.8 eV) as a reference.

The photoluminescence emission spectra (PL) of samples were analyzed on a fluorescence spectrophotometer (Hitachi, Model F-7000) with an excitation wavelength of 240 nm at room temperature. The photocurrent was carried out by using a three electrodes cell. The resultant FTO electrodes including the catalysts were served as the working electrode with a platinum wire as the counter electrode and an Ag/AgCl (saturated KCl solution) electrode as the reference electrode.

2.3. Catalytic performances

The catalytic performances of this catalyst samples for NO reduction by CO were conducted in a fixed-bed flow micro-reactor under an atmospheric pressure. In the typical reaction, the catalyst (500 mg) with a grain size of 0.2–0.3 mm was packed in a flat-plate quartz cell (30 × 20 × 0.5 mm) (ensuring the interaction of light and the majority sample, seeing Fig. S1 in Supplementary information (SI)) and heated by an electric resistance board. The temperature of the catalyst bed was monitored by a K-type thermocouple inserted into the reactor. During the photo-thermal reaction process, visible light (produced by a 300 W xenon lamp with a visible light-reflectance filter, 420 nm < λ < 760 nm) was irradiated from the top surface of the quartz cell. As testing the pure thermal reactions (without light), the quartz cell was enclosed by Al foils to rule out light irradiation. The feed stream (composition: 1500 ppm NO, 1500 ppm CO, and the balance gas He) was fed at a total flow rate of 100 mL min^{-1} (GHSV = 20,000 h^{-1}). Before introducing the reaction gas stream into the reaction system, the

catalyst samples were first pretreated in 5.0 vol% H_2–He atmosphere at 120 °C for 2 h with the flow rate 70.0 mL min^{-1}. Then the H_2–He stream was switched to the pure He stream, until the temperature was cooled down to room temperature. Finally, the feed stream (CO + NO) was switched into the reaction system and the catalytic activities were performed under feed stream at a series of temperatures (60, 80, 100, 120 and 140 °C), respectively. After reacting for 2 h at each temperature in the dark, the visible light was introduced into the reactor for another 2 h. The effluent stream was analyzed by an online NDIR NO_x-analyser (OW/AI300, ONUEE). The NO conversion, CO conversion and N_2 selectivity were calculated as follow, respectively:

$$\text{NO conversion} = \frac{NO_{in} - NO_{out}}{NO_{in}}$$

$$\text{CO conversion} = \frac{CO_{in} - CO_{out}}{CO_{in}}$$

$$N_2 \text{ selectivity} = \frac{2N_{2out}}{NO_{in} - NO_{out}}$$

2.4. CO and NO adsorption measurement by in-situ DRIFTS

In-situ DRIFTS were collected on a Thermo Fisher Scientific IS50 FT-IR instrument equipped with a high-sensitivity MCT detector (cooled by liquid N_2 at 77 K). The spectra were recorded from 1000 to 4000 cm^{-1} at a spectral resolution of 4 cm^{-1} (the times of scans at 64). The DRIFTS cell (Harrick) was fitted with two ZnSe windows and heating cartridge, which allowed the samples to be heated to 600 °C. Prior to each experiment, the samples were pretreated in pure He streamat 400 °C for 1 h to eliminate the other impurities. The samples' background spectra of each target temperature were collected during the cooling process, respectively. After cooling down to ambient temperature, the samples were exposed to a controlled stream of 5000 ppm CO or 5000 ppm NO in He for 30 min to be saturated. Then all of the spectra were obtained by subtraction of the corresponding background reference. For comparison, the visible light irradiated the samples at the identical temperature by a 100 W high-pressure mercury lamp through a quartz window located on the dome of DRIFTS cell.

3. Results and discussion

3.1. Catalyst characterization

3.1.1. Structure properties

The XRD patterns of $LaFeO_3$ and Pd-$LaFeO_3$ samples in Fig. 1 show that $LaFeO_3$ presents the structure of standard orthorhombic perovskite phase [22] (reflection peak at 2θ of 22.63°, 32.22°, 39.73°, 46.21°, 52.04°, 57.45°, 67.42°, 72.12°, 76.69°) except a weak diffraction peak at 29°, which could be indexed to the (011) reflection of hexagonal La_2O_3 (JCPDS card no. 83-1344), indicating a trace of La_2O_3 in $LaFeO_3$. But it disappeared because of a deposition precipitation with $PdCl_2$ dissolved in hydrochloric acid. Also, the characteristic diffraction peaks of Pd species were not observed in the XRD pattern of Pd/$LaFeO_3$. This may be due to the low content or/and a high dispersion of Pd nanoparticles in Pd/$LaFeO_3$ sample. In addition, the mean crystallite size of $LaFeO_3$ calculated by Scherrer formula was about 18 nm, while loading palladium could cause the slight decrease in the crystallite size (seeing Table 1).

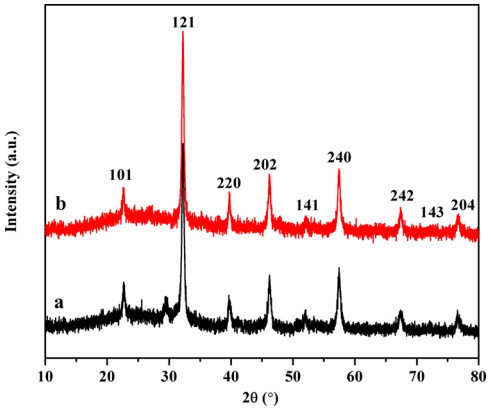

Fig. 1. XRD patterns of (a) $LaFeO_3$ and (b) Pd/$LaFeO_3$ samples.

It is well known that gas–solid reactions generally take place at catalyst surface. Consequently, the understanding of more surface information of samples is very significant. Raman spectrum is an effective method for further detecting the interaction of metal oxides for obtaining some additional structure information, which cannot be obtained by XRD. As can be seen in Fig. 2, the Raman spectrum of $LaFeO_3$ sample exhibited a band with the frequency at 141 cm^{-1} corresponding to the A_g vibration model of La cation [28–30]. The band observed around 272 cm^{-1} was assigned to the oxygen of FeO_6 octahedra tilt (T) modes [30]. The scatterings observed at 430 cm^{-1} were associated to B_{3g} bending vibrations mode (B) of octahedral Fe–O and 655 cm^{-1} consistent with the oxygen stretching vibrations (S) [29,30]. In particular, 1154 cm^{-1} was assigned to the one phonon scattering [31], while the intense and broad band around 1311 cm^{-1} in $LaFeO_3$ sample could be ascribed to second-order excitation of the 655 cm^{-1} band [30]. All the defined peaks were attributed to orthorhombic perovskite structured $LaFeO_3$ except the weaker observed at 210 cm^{-1} assigned to trace of Fe_2O_3 [7].

Nevertheless, in comparison with the pure $LaFeO_3$ sample, it was observed that the peaks located at 141, 210, 272, 1154 and 1311 cm^{-1} remained unchanged without a significant shift after loading Pd nanoparticles. Interestingly, the band at 655 cm^{-1} made a clear red shift to 592 cm^{-1} accompanied with a slight decrease of its intensity, indicating that Pd nanoparticles may weaken the intensity of Raman stretching on Fe–O bond and closely contact with Fe–O bond of crystallite $LaFeO_3$ to form a new Fe–O–Pd bond. Moreover, the peak at 430 cm^{-1} involved in bending mode in octahedron of $LaFeO_3$ also made a red shift to 420 cm^{-1}. This decrease of frequency may be related to the substitution of Fe ions by the heavier Pd ions which enhanced the average mass of the B site cation. Because the frequencies of the Raman modes are dependent on force constant and ionic mass (the heavier atoms vibration at the lower frequencies) [32].

Therefore, the differences between both spectra were associated with the introduction of Pd into the surface or lattice of $LaFeO_3$, which may provide a physical basis for highly efficient electron transfer and be responsible for the higher activity. In additional, Kim et al. [21,33] also substantiated that Pd substituting for perovskite oxide B sites also improved thermal stability of catalysts and prevented noble metal sintering phenomena that reduced the performance of automotive catalysts in the high temperature.

3.1.2. Texture characteristics

Fig. 3 exhibits the N_2 adsorption–desorption isothermal plots and the corresponding BJH pore size distribution curves of as-prepared samples. The observed isotherms shown in it were identified as type IV with a type H1 hysteresis loop as defined by IUPAC, which indicated the mesoporous feature of the $LaFeO_3$ product. The textural parameters of the samples are also summarized in Table 1. The BET specific surface area of $LaFeO_3$ was 23.7 $m^2 g^{-1}$ with a pore volume of 0.13 $cm^3 g^{-1}$. However, as compared to pure $LaFeO_3$, when loading Pd on $LaFeO_3$, both the specific surface area (74.8 $m^2 g^{-1}$) and pore volume (0.38 $cm^2 g^{-1}$) increased, which may be beneficial for the adsorption of CO and NO during the reaction process.

3.1.3. Surface morphology of prepared catalysts

The microstructure and morphology of the synthesized samples

Table 1
The results of texture properties of $LaFeO_3$ and $Pd/LaFeO_3$ samples.

Samples	Surface area ($m^2 g^{-1}$)	Pore volume ($mL g^{-1}$)	Pore diameter (nm)	Particle size (nm)	Band gap (eV)
$LaFeO_3$	23.60	0.13	24.53	18.29	2.13
$Pd/LaFeO_3$	74.80	0.38	21.38	17.32	2.02

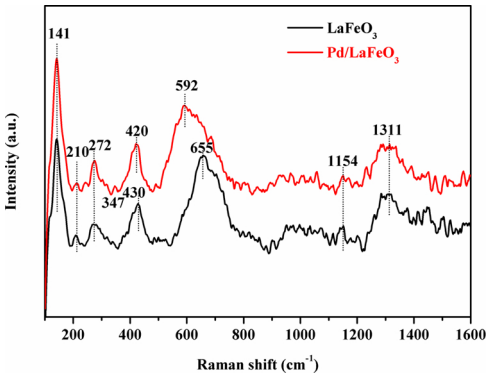

Fig. 2. Raman spectra of $LaFeO_3$ and $Pd/LaFeO_3$ samples.

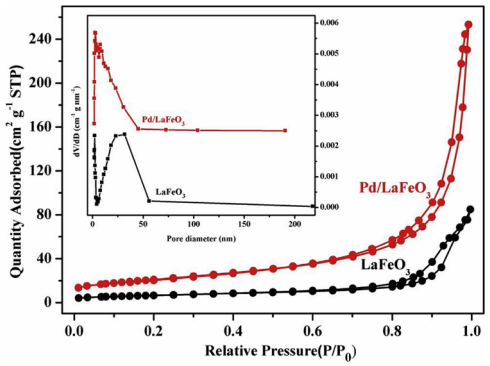

Fig. 3. The N_2 adsorption–desorption isotherms and corresponding pore size distribution curves (inset) of $LaFeO_3$ and $Pd/LaFeO_3$ samples.

were further characterized by SEM. As shown in Fig. 4(a) and (b), both $LaFeO_3$ and $Pd/LaFeO_3$ samples consisted of the stack of uniform nanoparticles with homogeneous arrays, which were cellular materials. The accumulation of the nanoparticles was also very incompact and there must be the significant porosity on the sample surface, which may be conducive to the catalytic activity through improving the dispersion of the active component and providing more adsorption sites. Furthermore, the loading of Pd could make the surface of $LaFeO_3$ nanoparticle rougher, which maybe created more favorable states to adsorb guest molecules and accelerate surface catalytic reactions. In addition, the high-resolution TEM image of $Pd/LaFeO_3$ in Fig. 4(c) showed that the Pd nanoparticles with (111) lattice plane (the lattice fringe with *d*-spacing of 0.227 nm) [34] were dispersed on the surface of $LaFeO_3$ support. Moreover, the interplanar spacing of 0.27 nm indexed to the (121) lattice plane of perovskite-type $LaFeO_3$ [35] was also observed. Additionally, the TEM image in Fig. 4(c) displayed a firm contact and a formed matching interface between Pd and $LaFeO_3$, which may facilitate the electron transfer between $LaFeO_3$ to and Pd nanoparticles, then lead to the enhancement of the photo-generated electron–hole pairs separation.

The chemical composition of $Pd/LaFeO_3$ composites was further analyzed by a EDS test. As shown in Fig. 4(d), numerous well-defined peaks of La, Fe and O were detected. The percentage of Pd remained in the final composite product was *ca.* 1.03 wt%, basically consistent with the theoretical value of Pd loading amount. In addition, a weak peak related to the signature from Au element and a strong C peak also included in the spectrum were due to sample coating material and electrical latex of TEM sample holder, which hence could be neglected for this sample. The EDS results clearly revealed that no impurity in the as-synthesized sample.

3.1.4. UV–vis diffuse reflectance spectra

Fig. 5 shows the DRS results of different samples. It was observed

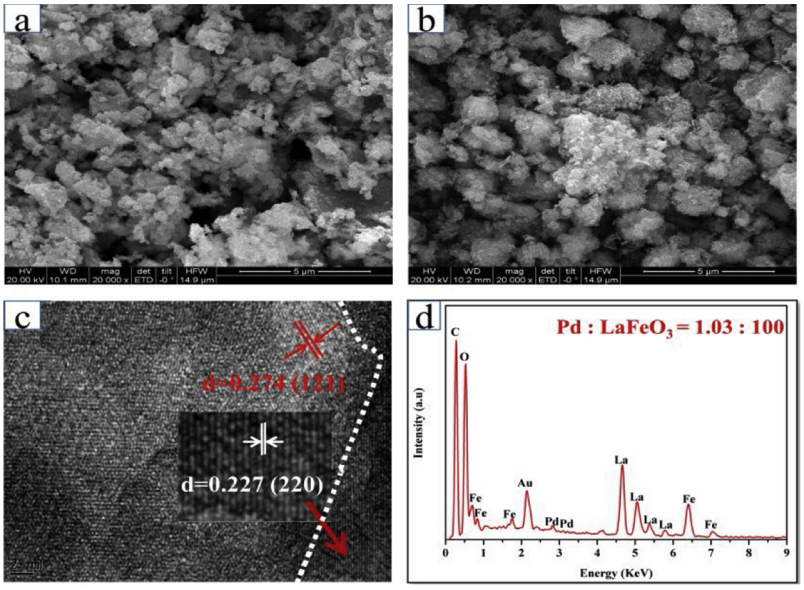

Fig. 4. SEM images of (a) $LaFeO_3$ and (b) 1.0 wt% $Pd/LaFeO_3$ samples; (c) TEM image of 1.0 wt% $Pd/LaFeO_3$ sample and (d) its EDS element analysis from TEM.

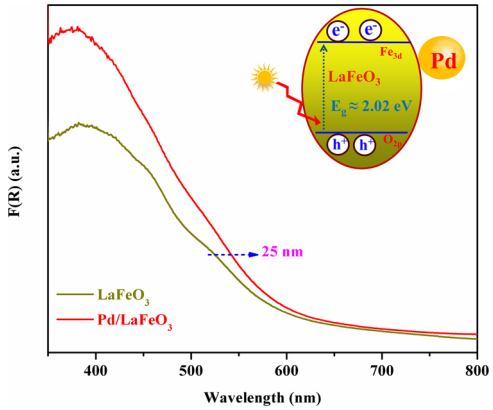

Fig. 5. UV–vis diffuse reflection spectra of $LaFeO_3$ and $Pd/LaFeO_3$ samples.

that $LaFeO_3$ showed an excellent visible light absorption edge at wavelength of around 590 nm (attributed to the characteristic absorption of $LaFeO_3$) [22]. The strong absorption could be generally related to the electronic transition from the valence band to conduction band (from O_{2p} to Fe_{3d} orbit, seeing the inset in Fig. 5) of $LaFeO_3$ sample [22]. However, the absorption edge of Pd loaded $LaFeO_3$ shifted slightly toward red region (up to *ca.* 615 nm) with an enhanced intensity of light absorption, indicating that loading Pd onto $LaFeO_3$ would broaden the light absorption region and enhance its absorption ability. The band gaps for $LaFeO_3$ and $Pd/LaFeO_3$ samples estimated from the Tauc plots of $(\alpha h\nu)^2$ versus photo energy ($h\nu$) [36] were 2.13 and 2.02 eV, respectively (seeing Fig. S2 in SI), which were similar to the reported value [22,23] and also summarized in Table 1.

3.2. Catalytic performances

Fig. 6 shows the performances of $LaFeO_3$ and $Pd/LaFeO_3$ for CO + NO reaction at different temperature under visible light irradiation or not. As can be seen in Fig. 6(a)–(c), with the increment of temperature, the CO conversion, NO conversion and N_2 selectivity were enhanced simultaneously. Moreover, the introduction of visible light could further enhance the CO conversion, NO conversion and N_2 selectivity over $Pd/LaFeO_3$, especially at the lower temperature (60 or 80 °C, with a poor activity in dark), indicating that visible light irradiation could promote the catalytic activities of $Pd/LaFeO_3$ for NO + CO reaction at low temperature. However, no apparent activity was exhibited for NO + CO reaction below 200 °C over the bare $LaFeO_3$ sample under visible light irradiation or not. Moreover, an inert Al_2O_3 (non-responsive to visible light) supported Pd nanoparticle sample (Pd/Al_2O_3) also did not exhibited a conspicuous photo-promoted catalytic effect for this reaction (seeing Fig. S3 in SI), indicating that it was the light excitation of $LaFeO_3$ support to be mainly responsible for the photo-assisted effect for the CO + NO reaction over $Pd/LaFeO_3$. Note that the as-prepared $Pd/LaFeO_3$ sample with a 1.0 wt% Pd content could fully exhibit the promoting effect of visible light for NO + CO reaction, although the increment at Pd content would enhance the catalytic activity of $Pd/LaFeO_3$ overall (seeing Fig. S4 in SI).

Furthermore, the $Pd/LaFeO_3$ sample was also applied to investigate the stability of catalytic performance at 120 °C for an interval of 20 h in light and dark. As seen in Fig. 7(a), the CO conversion over $Pd/LaFeO_3$ gradually decreased in dark with the prolonged reaction time. After introducing visible light into the reaction system, the CO conversion increased obviously but still gradually dropped down. Nevertheless, the NO conversion over $Pd/LaFeO_3$ almost kept stable under visible light irradiation or in dark (seeing Fig. 7(b)). The decrease in CO conversion as well as the stability of NO conversion meant the decrease of N_2 selectivity ($2CO + 2NO \rightarrow 2CO_2 + N_2$). Herein, more NO may be reduced to N_2O ($CO + 2NO \rightarrow CO_2 + N_2O$). These above results indicated that

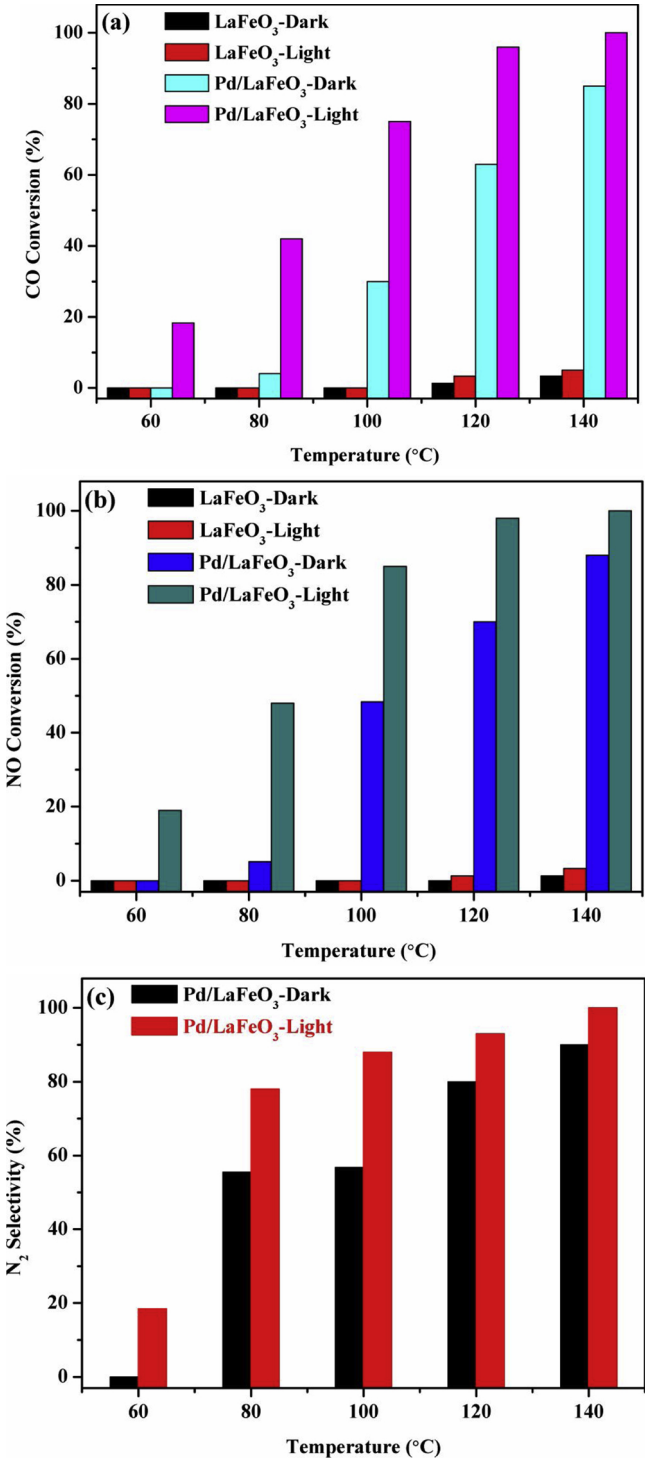

Fig. 6. CO conversion (a); NO conversion (b) and N_2 selectivity (c) at different reaction temperatures over $LaFeO_3$ and $Pd/LaFeO_3$ samples under visible light irradiation or in dark, respectively.

$Pd/LaFeO_3$ exhibited a higher catalytic activity and better stability of reducing NO to N_2 by CO under visible light irradiation. Moreover, the sustained high catalytic performance for CO + NO reaction over $Pd/LaFeO_3$ after 20 h tests also implied that $Pd/LaFeO_3$ itself had an excellent long-term photo-stability. In fact, the reacted $Pd/LaFeO_3$ sample exhibited a similar crystal and surface structure to that of the fresh sample by the XRD and Fourier Transform infrared spectroscopy (FTIR) results (seeing Fig. S5 in SI).

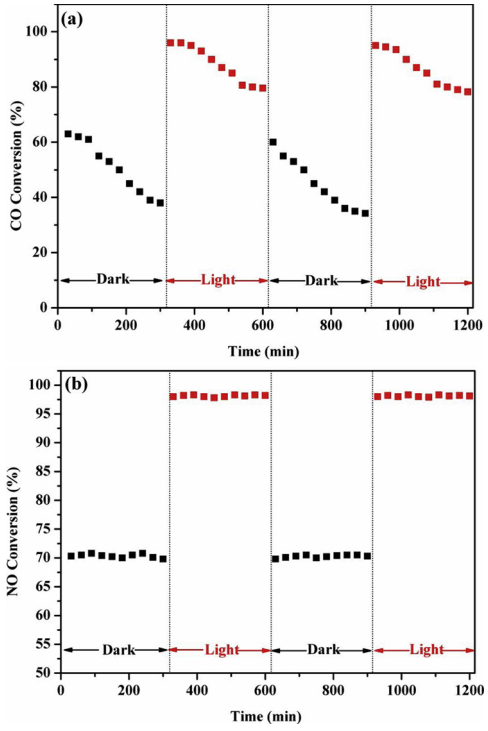

Fig. 7. Conversions of CO (a) and NO (b) as function of reaction time at 120 °C over Pd/$LaFeO_3$ under visible light irradiation or in dark, respectively.

3.3. Chemisorption behaviors of CO and NO

According to the thermo-catalytic reaction process of CO + NO [6–8], the adsorption and activation of reactant molecules on the catalysts surface would play vital effects on the reaction proceeding and the formation of intermediate active species. Our previous studies [12,15] also found that the light irradiation on Au or Pt loaded support surface could be favorable for the adsorption and activation of CO or NO, then accelerated their oxidation or reduction. To further explore the interaction of the catalyst sample and reactant molecules, the *in-situ* DRIFTS testing for adsorbing NO, CO and CO + NO over Pd/$LaFeO_3$ was also performed under visible light irradiation or in dark, respectively.

3.3.1. In-situ DRIFTS testing of CO adsorption

Fig. 8(a) and (b) shows the DRIFTS of adsorbing CO over Pd/$LaFeO_3$ sample at different temperatures under visible light irradiation or in dark. The assignment of these bands is given in Table 2. As seen in Fig. 8(a), for Pd/$LaFeO_3$ adsorbing CO at room temperature in dark, three obvious adsorption peaks were observed at 2170 cm^{-1}, 2094 cm^{-1} and 1948 cm^{-1}, which were assigned to the R-branch of gaseous CO [6], linear CO adsorption on Pd (111) and bridged CO adsorption on Pd (100) sites [33], respectively. Apparently, the intensity of CO adsorption peak at 2080 cm^{-1} was much stronger than that of peak at 1940 cm^{-1}, indicating that the CO linear adsorption on metallic Pd was the main adsorption mode over Pd/$LaFeO_3$ sample. Nevertheless, the vibration modes of bidentate carbonates (1590 cm^{-1}) and monodentate carbonate (1435 cm^{-1}) of CO adsorption on Fe^{3+} [7] were not detected in the DRIFTS, which further verified that the Pd was the primary adsorption site for CO. Moreover, a negative band observed at *ca.* 2350 cm^{-1}, which was attributed to the formation of chemically adsorbed CO_2 (*i.e.*, CO reacting with surface hydroxyls [37]) due to the CO adsorption, could be explained by the change at surrounding atmosphere environment (CO_2 and H_2O). Except for the peaks mentioned above, some peaks were also observed between 1000 cm^{-1} and 1800 cm^{-1}. The peak at about 1040 cm^{-1} was the vibration of

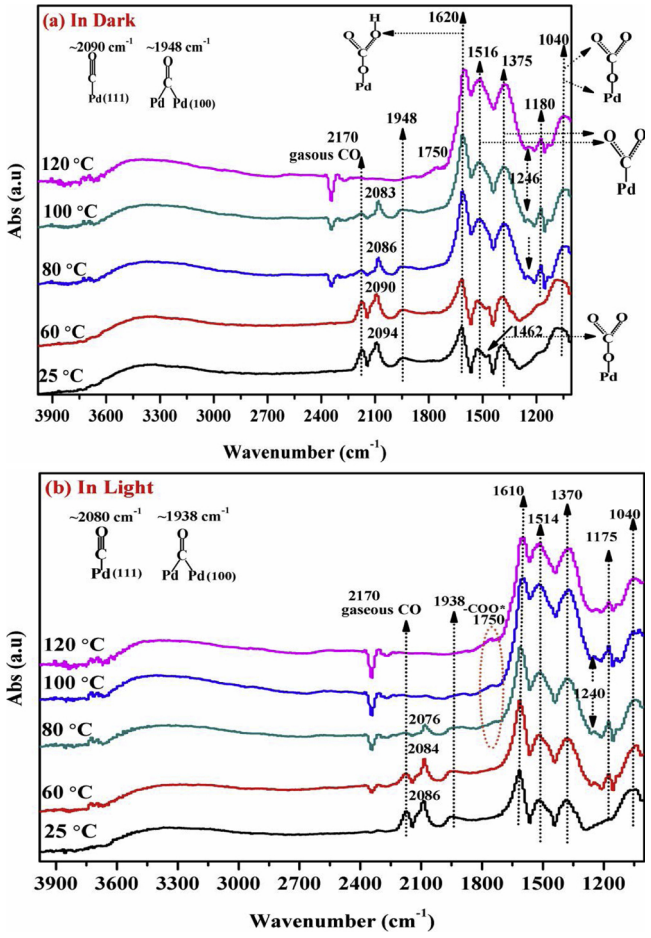

Fig. 8. DRIFTS spectra of adsorbing CO over Pd/$LaFeO_3$ samples at different temperatures, (a) in dark or (b) under visible light irradiation.

Table 2
Assignments of the DRIFTS bands observed during CO adsorption over Pd/$LaFeO_3$.

Wavenumber (cm^{-1})	Assignment	References
2350	Gaseous CO_2	[37]
2170	Gaseous CO	[6]
2094	Linear CO adsorption on Pd	[33]
1948	Bridged CO adsorption on Pd	[33]
1750	Carbonyl coupling vibration	[7]
1620	Hydrogen-carbonate group	[8,38]
1515	Anti-symmetric vibration mode of carboxylate	[7,39]
1460	Monodentate carbonate or free carbonate	[7,39]
1375	Symmetric vibration mode of carboxylate	[7,39]
1246, 1180	Stretching vibration of carbonyl	[40,41]
1040	Hydrogen carbonate species or the surface monodentate carbonates	[6,38]

hydrogen carbonate species or the surface monodentate carbonates, *i.e.*, *ν*(C–O) [6,38]. The other bands observed at *ca.* 1375, 1460, 1515, and 1750 cm^{-1} were assigned to symmetric stretching vibration mode of carboxylate radical, monodentate carbonate or free carbonate vibration, anti-symmetric vibration mode of carboxylate as well as carbonyl coupling vibration, respectively [7,39], which could derive from the result of the CO adsorption at Pd sites reacting with the adjacent lattice oxygen of $LaFeO_3$. An obvious band at 1620 cm^{-1} could be assigned to the vibration mode of hydrogen-carbonate groups [8,38] (maybe corresponding to the bending vibration mode of O–H bond in the hydrogen-carbonate structure). This formed hydrogen-carbonate species

induced by the adsorbed CO interacting with surface hydroxyls [15,37] could further be transformed into H_2O and CO_2, which exhibiting the well-known bending mode (*ca.*1620 cm^{-1}) and the stretching mode (seeing the bands at 3000–3600 cm^{-1} in Fig. 8(a)) of H_2O molecules. More importantly, with the increasing temperature up to 100 °C, the peak at 2080 cm^{-1} and gaseous CO peak at 2170 cm^{-1} disappeared gradually, while the peak intensity of 1940 cm^{-1} kept constant, indicating that the CO adsorption on the metallic Pd (111) would be first consumed then gradually transformed to some other carbonate, carboxylate or carbonyl intermediates located at wavenumber of 1000–1800 cm^{-1}, eventually into CO_2. Typically, with the process of raising temperature up to 60 °C, exactly the activated temperature of catalyst samples for the CO + NO reaction in dark, the band at 1462 cm^{-1} disappeared and 1040 cm^{-1} gradually decreased while peaks at 1620 and 1375 cm^{-1} gradually enhanced. Simultaneously, the new band at 1180 cm^{-1} and a weak peak at 1246 cm^{-1} indexed to the C–O stretching vibration of carbonyl [40,41] were also observed. It suggested that as the reaction proceeding, the monodentate carbonate would transform to the other species containing carbonyl (*e.g.*, COO–), while more bicarbonate might stem from the more adsorbed CO interaction with surface hydroxyls species. However, all the above three CO bands would be vanished absolutely as the temperature above 100 °C. These phenomena clearly illustrated that gaseous CO and adsorbed CO at Pd sites could directly react with the catalyst sample, *i.e.*, surface hydroxyl group or the lattice oxygen atom.

However, with respect to the CO adsorption under visible light irradiation at the identical condition (seeing Fig. 8(b)), no obvious new peaks were detected, which also indicated that the existed strong interaction between CO species and catalyst sample although in dark. Nevertheless, some new events would be observed all the same. Compared to the adsorption process in dark, the consumption of gaseous CO and chemisorbed CO was more apparent. Just at 100 °C the bands of CO vanished completely. Furthermore, the peak at 1462 cm^{-1} ascribed to monodentate carbonate got much weaker than it in dark, indicating that it could be transformed to other intermediates effortlessly after introducing visible light. Simultaneously, the peaks at 1175 cm^{-1}, 1240 cm^{-1}, 1610 cm^{-1} and 1750 cm^{-1} came to occur also at the lower temperature and wavenumbers. It was worth noting that the CO-Pd (111) and CO-Pd (100) adsorption sites shifted to a lower wavenumber as well (from 2094 to 2086 cm^{-1}, 1948 to 1938 cm^{-1}). These may be attributed to the higher surface electron density of Pd nanoparticles over Pd/$LaFeO_3$ than that of Pd in dark. Under visible light irradiation, more electrons (transferred from the $LaFeO_3$) in 5sp orbital of Pd could further transfer to the anti-bonding π^*-orbital of CO adsorption at Pd sites according by the principle of d–π^* back-donation (seeing Fig. 12(b)), resulting in a weaker C(O bond (*i.e.*, the C–O infrared stretching vibration frequency shifts to a lower frequency), then promoted the activation of CO molecule [15,42]. In additional, the CO adsorption behaviors over Pd/$LaFeO_3$ could be also confirmed by the CO-TPD test (seeing Fig. S6 in SI).

3.3.2. *In-situ DRIFTS testing of NO adsorption*

Fig. 9 depicts the *in-situ* DRIFTS of NO adsorption on the Pd/$LaFeO_3$ at the varied temperatures under visible light irradiation or in dark. The assignment of these bands is listed in Table 3. As seen in Fig. 9(a), exposing Pd/$LaFeO_3$ to NO stream at room temperature led to a much weaker gaseous NO band detected at *ca.* 1905 cm^{-1} [6] and the emergence of some peaks in the range of 1000–1900 cm^{-1}, which indicated that NO species were strongly adsorbed on sample surface. While the inapparent peak at 1750 cm^{-1} viewed as being characteristic of NO linearly bonded on the Pd^0 (111) [24,43] affirmed that the NO was mainly adsorbed on $LaFeO_3$ support surface rather than Pd sites at low temperature. Moreover, the bridging bidentate nitrates adsorption displayed a $–NO_2$ symmetric vibration mode at 1020 cm^{-1} and a N═O stretching mode at 1610 cm^{-1} [6,44]. Moreover, Lobree et al. [45] also reported that the bands about at 1600 cm^{-1} could be indexed to nitro

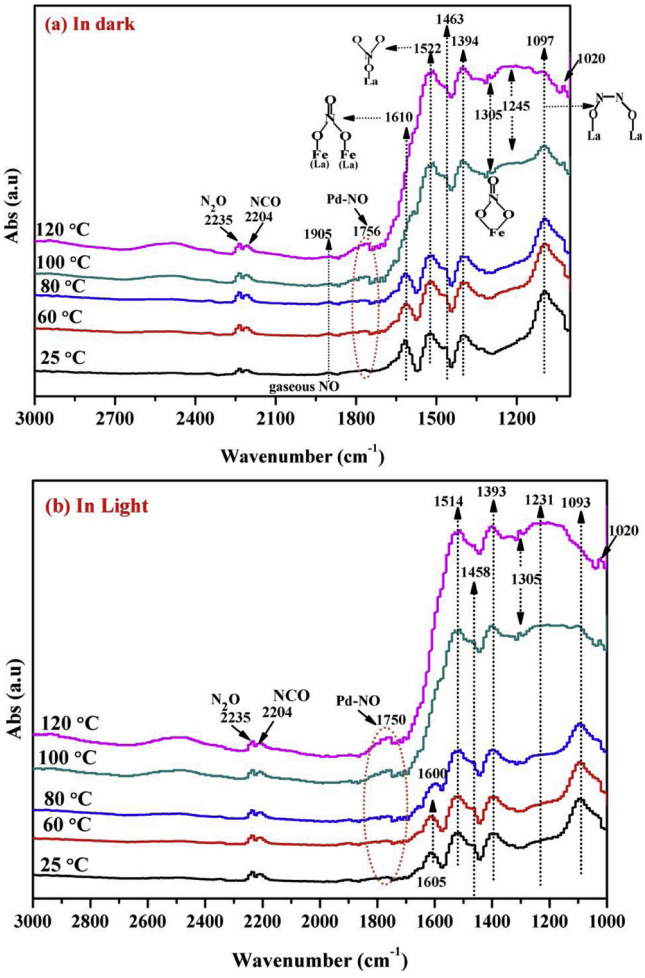

Fig. 9. DRIFTS spectra of adsorbing NO over Pd/$LaFeO_3$ samples at different temperatures, (a) in dark or (b) under visible light irradiation.

Table 3
Assignments of the DRIFTS bands observed during NO adsorption over Pd/$LaFeO_3$.

Wavenumber (cm^{-1})	Assignment	References
2235	N_2O	[15]
2204	–NCO	[15]
1905	Gaseous NO	[6]
1750	NO linearly bonded on the Pd	[24,43]
1610	Bridging bidentate nitrates	[6,44]
1522	Unidentate nitrate on La^{3+} or chelating bidentate nitrate	[8,46]
1463	Bridging monodentate nitrate	[47]
1394	Free nitrate species	[8]
1305	Chelating bidentate nitrate on Fe^{3+}	[47]
1245	Chelating bidentate nitrite or unidentate nitrate on	[8]
1097	Hyponitrite ion $N_2O_2^{2-}$ (cis) on La	[46]
1020	Bridging bidentate nitrates	[6,44]

group associated with and Fe^{n+} cation, which further indicated that the NO mainly adsorbed on the $LaFeO_3$ sites. Additionally, the observed peaks at 1522, 1463, 1394, and 1093 cm^{-1} could be attributed to the different types of nitrates adsorbed at different sites or in different geometry. Herein, the peak at 1522 cm^{-1} could be ascribed to the unidentate nitrate on La^{3+} [46] or chelating bidentate nitrate [8], 1463 cm^{-1} to the bridging monodentate nitrate [47], 1394 cm^{-1} to free nitrate species [8] and 1097 cm^{-1} to hyponitrite ion $N_2O_2^{2-}$ (cis) on La [46]. In addition, note that two peaks at 2204 cm^{-1} and

2235 cm^{-1} [11,15] respectively attributed to isocyanate –NCO and N_2O were also detected, implying the adsorbed nitrogen oxide maybe reacted with the surface residual carbonaceous species, generating few –NCO intermediates. The slight N_2O emergence at low temperature could be explained by the partially decomposition of nitro species 2NO (g) → 2NO (ad) → N_2O (g) + O (ad) [7,47].

Apparently, as the reaction temperature increment, the increasing peak at 1756 cm^{-1} indicated that the higher temperature could promote the NO adsorption at the Pd sites (the increased peak at *ca.* 1750 cm^{-1} maybe also originating from dinitrosyl complex due to the strong adsorption of NO [43]). Moreover, the peaks of 1610 cm^{-1} and 1093 cm^{-1} stepwise decreased then disappeared absolutely at 120 °C, but the band at 1522 cm^{-1} increased accompanied with the appearance of bands at 1305 cm^{-1} (chelating bidentate nitrate on Fe^{3+}) [47] and 1245 cm^{-1} (chelating bidentate nitrite [8] or unidentate nitrate on La^{3+} [46]), demonstrating that the bridging bidentate nitrate and hyponitrite ion $N_2O_2^{2-}$ as the key intermediates would interact and transform to chelating types nitrate and unidentate nitrate when temperature rising. These above results all indicated that Pd/$LaFeO_3$ sample could adsorb and activate NO vigorously. Moreover, similar to CO adsorption on catalyst samples, no new peak could be observed over Pd/$LaFeO_3$ with the introduction of visible light except that the peaks shifted red somewhat and were decreased obviously at the identical temperature. The peaks corresponding to the Pd-NO, bridging bidentate nitrates, chelating bidentate nitrate and monodentate nitrate all shifts to a lower wavenumber (from 1756, 1610 and 1522 cm^{-1} to 1750, 1600, and 1514 cm^{-1}, respectively, seeing Fig. 9(b)) under visible light irradiation. This meant that visible light irradiation could further weaken the respective vibration of the adsorbed NO-contained species at Pd or $LaFeO_3$ support due to the back-donation of the d-electron from the metal cation to the anti-bonding orbital of NO [6]. Therefore, also as the *in-situ* DRIFTS as CO adsorption, maybe the introduction of visible light indeed would promote the electron transfer between $LaFeO_3$ and Pd, resulting in the increase in the surface electron density of Pd and Fe sites and providing the foundation of the adsorption and activation of NO.

3.3.3. Co-adsorption of NO and CO over Pd/$LaFeO_3$ sample

To further disclose the behavior of visible light irradiation on the reaction of NO + CO over Pd/$LaFeO_3$, the *in-situ* DRIFTS studies of catalyst samples co-adsorbing NO and CO were performed at room temperature, 60 °C (the Light-off temperature) and 120 °C under visible light irradiation or not. As shown in Fig. 10 and Table 4, exposing Pd/$LaFeO_3$ to NO + CO streams at room temperature led to the emergence of some IR bands in the range of 1000–2500 cm^{-1}, corresponding to the different active species adsorbed on the surface of catalyst, such as NO linearly adsorption on Pd^0 (1735 cm^{-1}) [24], hydrogen-carbonate or bridging bidentate nitrates (1620 cm^{-1}) [38,44], 1355 for ionic nitrate species on Fe^{3+} [47], 1100 cm^{-1} for cis-N_2O_2 on La sites [46],

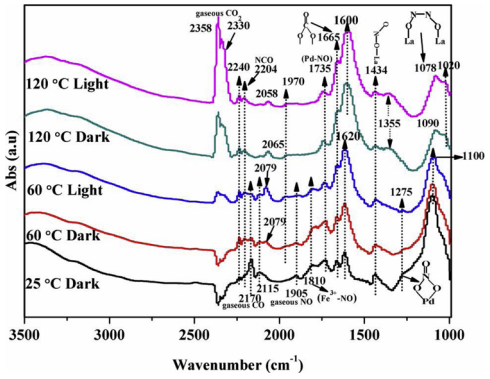

Fig. 10. DRIFTS spectra of co-adsorbing CO and NO over Pd/$LaFeO_3$ samples at different temperatures, (a) in dark or (b) under visible light irradiation.

Table 4
Assignments of the DRIFTS bands observed during CO + NO adsorption over Pd/$LaFeO_3$.

Wavenumber (cm^{-1})	Assignment	References
2358, 2330	CO_2	[37]
2240	N_2O	[15]
2204	–NCO	[15]
2115, 2170	Gaseous CO	[6]
2079, 1970	Linear or bridged adsorption CO on Pd	[33]
1905	Gaseous NO	[6]
1810	NO adsorbed on Fe^{3+}	[48]
1735	NO linearly bonded on the Pd^0	[24,43]
1665	Bidentate carbonate	[7]
1620	Bridging bidentate nitrates	[44]
1434	Bridging monodentate nitrites	[46]
1355	Ionic nitrate species on Fe^{3+}	[47]
1275	Chelated nitrate on Pd	[47]
1100	Cis-N_2O_2 on La sites	[46]
1020	Bridging bidentate nitrates	[6,44]

1275 cm^{-1} for chelated nitrate on Pd weakly [47], 1020 cm^{-1} for –NO_2 symmetric vibration of bridging bidentate nitrates [6,44]. In addition, P-branch and R-branch of gaseous CO (2115 and 2170 cm^{-1}), the negative peaks at 2358 and 2330 cm^{-1} assigned to the physisorbed CO_2, gaseous NO (1905 cm^{-1}) [6] were observed in the region of recorded spectrum at 25 °C as well. However, different from the single CO or NO adsorption on as-prepared sample, the peaks at 1516, 1375 cm^{-1} (ascribed to carboxylate) and 1522 cm^{-1} (ascribed to unidentate nitrate or chelating bidentate nitrate) could not be observed in the spectrum of co-adsorption. Meanwhile, the emergence of new peaks at 1665 cm^{-1} indexed to bidentate carbonate [7], 1434 cm^{-1} to bridging monodentate nitrites [46,47] and 1810 cm^{-1} to the NO adsorbed on Fe^{3+} [48] indicated that activated carboxylate would directly interact with unidentate nitrate to form higher oxidized carbonate and lower oxidized monodentate nitrites, while CO as a reductive gas boosted NO adsorption at Fe sites at low temperature.

Moreover, as the reaction temperature up to 60 °C, the gaseous CO and NO stepwise decreased then transformed to the linear or bridged adsorption CO on Pd sites at 2079 and 1970 cm^{-1}, NO on $LaFeO_3$ sites at 1620 cm^{-1}, respectively. In addition, as compared to the case of Pd/$LaFeO_3$ adsorbing CO, NO and CO + NO in dark (seeing Figs. 8(a), 9(a) and 10), the introduction of visible light irradiation at 60 °C could lead to the increase in CO adsorption bands at 2079 and 1970 cm^{-1}, NO adsorption peaks at 1620 cm^{-1}, the generation of new CO_2 species (2358 and 2330 cm^{-1}) and slight N_2O (2240 cm^{-1}) species. This meant that visible light irradiation could further promote adsorbed CO and NO to be activated over Pd/$LaFeO_3$ then interact to form CO_2, N_2O and N_2. In fact, Weisweiler et al. [49] and Lv et al. [8] reported the N_2O was also considered as an intermediate of CO + NO reaction (CO + N_2O → CO_2 + N_2). However, as the reaction temperature up to 120 °C, all the CO and NO adsorption peaks decreased obviously accompanied with the increasing CO_2 species and constant N_2O, disclosing that the higher temperature would be favorite for the reduction of NO by CO and improve the selectivity of N_2, consistent with the results of activity testing. Furthermore, with the introduction of visible light, the peaks of Pd-CO, bridging bidentate nitrate and cis-$N_2O_2^{2-}$ shifted to the lower wavenumber (from 2065, 1620 and 1090 cm^{-1} to 2058, 1600, and 1078 cm^{-1}, respectively) accompanied with the more CO_2, further indicating that visible light indeed promoted the activation of CO and NO adsorbed at Pd or $LaFeO_3$ sites.

However, compared to Pd/$LaFeO_3$ adsorbing single NO under visible light irradiation or not, the continuously decreasing cis-$N_2O_2^{2-}$ at La sites (1100 cm^{-1}), unchanged chemisorbed NO at Pd sites (1735 cm^{-1}) and increasing bridging bidentate nitrates at Fe sites (1600 cm^{-1}) indicated that in the case of co-adsorption, CO would preferentially interact with cis-$N_2O_2^{2-}$ (the lower oxidation state of N

atom) while be beneficial to the adsorption of NO at Fe sites, for the preferential adsorption of CO at Pd sites maybe suppressed the adsorption of NO at Pd sites. Note that the –NCO species (2204 cm^{-1}) [8,15] over Pd/$LaFeO_3$ after co-adsorbing CO and NO were also observed as the increase of temperature, indicating that the –NCO intermediates would be produced during this reaction process. In fact, the –NCO species (Pt-CO + NO_{ads} → Pt-NCO + O_{ads}) was regarded as an important intermediate for NO reduction to N_2 [15]. Moreover, Ozensoy et al. [26] also reported that the generation of –NCO functional group on Pd (111) could be used as a sensitive indicator for the NO dissociation process, which was also the crucial indicator for the CO + NO catalytic reaction [6–8]. However, the peak of –NCO species did not increase with the introduction of visible light in Fig. 10, indicating that the formation of –NCO species may not be the rate-determining step for this reaction over Pd/$LaFeO_3$. It may be the adsorption and activation of NO at Fe or La site to be mainly responsible for this reaction.

Therefore, based on the above *in-situ* DIRFTS results, it could be arrived at conclusions as follows: (1) Visible light irradiation could promote the adsorption and activation of CO at Pd sites and that of NO at La or Fe sites over Pd/$LaFeO_3$. (2) The presence of NO promoted the CO activation into carbonate while CO maybe enhanced the adsorption of NO at Fe sites as well as promoted the NO activation into monodentate nitrites, which could be further promoted by visible light irradiation. (3) With the reaction proceeding, the CO linearly bonded on Pd sites would preferentially react with cis-$N_2O_2^{2-}$ adsorbed on La sites due to its lower oxidized state, and also benefit to the formation of intermediate species of NO adsorption such as bridging bidentate nitrate. (4) The formation of –NCO (as an important intermediate species for NO reduction to N_2) and promoted generation of CO_2 species with constant N_2O over Pd/$LaFeO_3$ further confirmed the positive effects of visible light irradiation for CO + NO reaction.

3.4. X-ray photoelectron spectroscopy (XPS) analysis

In our previous works [12–15], we have suggested that a higher surface electron density of Pt or Au would be favorable for the activation of CO species adsorbed at its surface, and then promoted the oxidation of CO over Pt/TiO_2 or Au/TiO_2. Combining with the results of chemisorption testing for CO and NO, for the reaction of NO + CO over Pd/$LaFeO_3$ under visible light irradiation, it was also proposed that the increase in Pd surface electron density induced by the effective charge transfer from $LaFeO_3$ would promote the adsorption and activation of NO and CO. To further confirm this viewpoint, the surface electron density of catalyst samples under visible light irradiation or not was studied via a XPS (the lower binding energy (BE) value means the higher surface electron density).

Fig. 11(a) shows the high-resolution XPS spectra of La3d of Pd/$LaFeO_3$ sample under different treatment conditions. The two peaks situated at about 834.8 eV ($3d_{5/2}$) and 851.4 eV ($3d_{3/2}$) indicated that La was predominately presented as La^{3+} state [50]. Besides, the XPS signals of La3d exhibited a typical double splitting (satellite lines on the higher binding-energy side of the 3d levels), which could be ascribed to the interaction of spin-orbit and the electron transfer from the oxygen valence band to the empty La4f level [50,51]. This result indicated that the electron interaction also existed between La and O atom over Pd/$LaFeO_3$. As compared to the fresh Pd/$LaFeO_3$ sample, the La $3d_{3/2}$ and $La3d_{5/2}$ peaks of Pd/$LaFeO_3$ catalysts shifted toward lower BE after reacted in dark but made a high shift after reacted in light process. The alternative surfaced electron density of La3d meant that La^{3+} also participated in the electron transfer during the photo-thermal coupling process.

Fig. 11(b) depicts the XPS results of O1s of Pd/$LaFeO_3$ sample under different treatment conditions. Each sample exhibited two apparent peaks of O1s at 529.3 and 531.0 eV, which were assigned to the lattice oxygen (O_L) and the surface chemisorbed hydroxyl groups or hydroxides (O_{ad}), respectively [13]. As compared to the fresh Pd/$LaFeO_3$ sample, the two O1s BE values of O_L and O_{ad} species over the reacted sample in dark made a positive shift of 0.4 eV (from 529.3 to 529.7 eV) and 0.6 eV (from 531.0 to 531.6 eV), respectively, However, the reacted sample under visible light irradiation exhibited a lower BE of O1s than the reacted sample in dark (O_L from 529.7 to 529.5 eV, O_{ad} from 531.6 to 531.2 eV), which was still higher than that of the fresh sample. These results indicated that the reaction process would decrease the electron density of surface oxygens (O_L and O_{ad}) either under visible light irradiation or not but visible light irradiation seemed somewhat to compensate electrons to the surface oxygen. Since the formation of oxygen vacancies could be related to consumption of O_{ad} (hydroxyls) [10,12,13] and cause the decrease in electron density of O_L [52] over TiO_2. The decreased electron density of surface oxygen over Pd/$LaFeO_3$ during the CO + NO reaction process could be also attributed to the formation of surface oxygen vacancies. The formed oxygen vacancies maybe effectively activated the N–O bond of the adsorbed NO species and then facilitated its reduction [6,7].

Note that the ratio of O_{ad} species (hydroxyls) to O_L over Pd/$LaFeO_3$ would decrease drastically after the reaction process in dark (seeing Table 5) as compared to that of fresh sample, indicating that some surfaced hydroxyl groups could be consumed (reacting with CO to form other active intermediates and final the CO_2 gas), consistent with the results of CO chemisorption (seeing Fig. 8 and Fig. S6 in SI).

However, the increase of this O_{ad}/O_L in light reaction than that in dark reaction meant that the photo-excitation of $LaFeO_3$ could promote the migration out of the lattice oxygen (forming oxygen vacancy and then the surface hydroxyls). Of course, the surfaced adsorbed CO or NO at sample maybe also directly reacted with the lattice oxygen to formed more activated intermediates (*e.g.*, carbonates, carboxylates, nitrate and nitrite species), resulting in the decrease in O_L.

The above explanation could be further confirmed by the XPS results of Fe2p in Pd/$LaFeO_3$ samples treated by different conditions. As shown in Fig. 11(c), Fe mainly existed in the state of Fe^{3+} (710.4 eV) and Fe^{4+} (712.4 eV) over all samples [53], The appearance of Fe^{4+} as an electrovalency compensation may be related to the existence of defect of Fe^{3+} cation, which was supported by the H_2-TPR results of $LaFeO_3$ and Pd/$LaFeO_3$ samples (seeing Fig. S7 in SI). Moreover, the surface atomic ratio from XPS also revealed that the Fe/La atom ratio of the fresh Pd/$LaFeO_3$ (0.59, seeing Table 2) was much smaller than that of the stoichiometric $LaFeO_3$ (1:1), further indicating the existence of surface iron cation vacancies. In addition, the BE of Fe2p made a high shift (up to 710.7 and 713.0 eV, respectively) after reacted in dark but shifted to the lower value (down to 710.4 and 712.7 eV) again after reacted under visible light irradiation. The similar BE transformation of Fe2p to that of O1s further affirmed that Fe and O atoms always as an integral offered electron either in dark or light reaction. Note that after reacted in dark, the decrease in area ratio of Fe^{4+} 2p to Fe^{3+} 2p in Pd/$LaFeO_3$ (seeing Table 5) meant that –FeO_x– experienced an apparent process of releasing oxygen overall. Here, Fe^{4+} would capture heat-excited electrons to form Fe^{3+} accompanied with the formation of oxygen vacancy. Nevertheless, the decreased ratio of Fe^{3+} to Fe^{4+} implied that –FeO_x– experienced the process of oxygen storage again when visible light was introduced into the above reaction process. Meanwhile, the lower Fe2p BE value (710.4 and 712.7 eV) for the reacted sample in light indicated the increase in surface electron density of Fe atom site, which may be related to the excitation of electron from O2p orbit to Fe3d orbit under visible light irradiation. It was probably this process of constant storage/release oxygen (Fe^{4+}/Fe^{3+}) over Pd/$LaFeO_3$ induced by photo-thermal coupling process that ensured the high activity and stabilization of Pd/$LaFeO_3$ under visible light irradiation.

Fig. 11(d) shows the high-resolution XPS spectra of Pd3d of Pd/$LaFeO_3$ samples. It attested that Pd species mainly exhibited in the states of Pd^0 (335.3 eV) and Pd^{4+} (337.2 eV) [54] in the fresh samples. This higher abnormally oxidation state (337.2 eV) of Pd substantiated

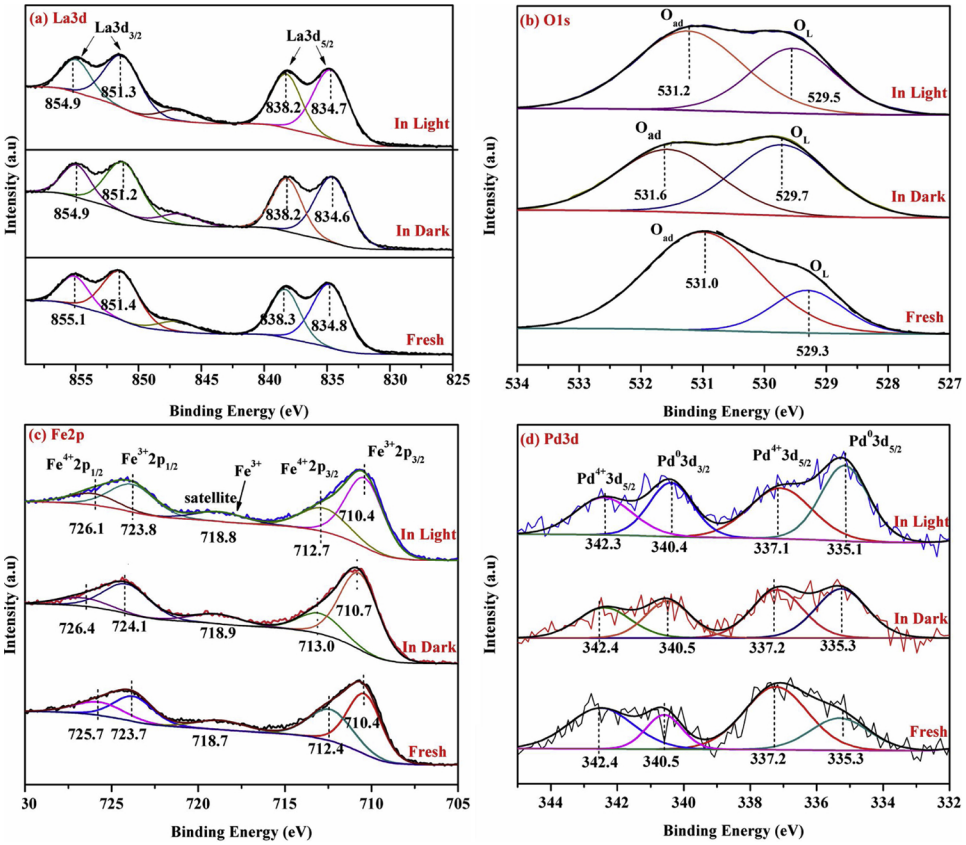

Fig. 11. High-resolution XPS spectra of La3d (a), O2p (b), Fe2p (c) and Pd3d (d) over Pd/$LaFeO_3$ samples under different treatments: (Fresh) after H_2 pre-treatment at 120 °C; (Dark) after reacted at 120 °C in dark; (Light) after reacted at 120 °C under visible light irradiation.

Table 5
Relative contents of surface species over Pd/$LaFeO_3$ samples under the different reaction conditions. (Fresh) after H_2 pre-treatment at 120 °C; (Dark) after reacted at 120 °C in dark; (Light) after reacted at 120 °C under visible light irradiation.

Samples	Atomic concentration			
	$O_{ad}/(O_{ad}+O_L)$ (at.%)	$Fe^{3+}/(Fe^{3+}+Fe^{4+})$ (at.%)	$Pd^0/(Pd^0+Pd^{4+})$ (at.%)	Surface atom ratios of Fe to La
Fresh	78.40	55.17	31.97	0.59
In dark	48.31	70.32	50.62	0.55
In light	60.42	64.49	52.79	0.54

that cationic Pd entities partially intercalated into the B-site of perovskite $LaFeO_3$ lattice as a solid solution [54,55] because of their similar radius and surface cation defects, consistent with the results of Raman spectra and the H_2-TPR profile (seeing Fig. S7 in SI). After reacted in the dark, Pd species still existed mainly in the state of Pd^0 and Pd^{4+} with a negligible BE change of Pd3d, indicating the surface electron density of Pd did not increase obviously in the process of sole heating reaction. Nevertheless, the apparently increased ration of Pd^0 (seeing Table 5) after reacted in the dark condition indicated that Pd^0 partially segregated and migrated out from $LaFeO_3$ lattice in the CO reductive atmosphere. In fact, Nishihata et al. [21] and Kim et al. [33] have ever reported that palladium of $LaFe_{0.57}Co_{0.38}Pd_{0.05}O_3$ catalyst was cycled involving a self-regeneration process at different atmospheres, typically encountered in exhaust gas owning to the strong interaction of Pd with the perovskite structure. Under a reducing environment Pd would move out of the perovskite structure then became the metallic Pd while fully dissolving into the its structure under an oxidizing condition, which could improve the catalyst thermal stability.

However, for the sample reacted under visible light irradiation, the BE of Pd3d was lower (335.1 eV and 337.1 eV) than that in dark. This meant that visible light irradiation could effectively promote the accumulation of surface electrons at Pd sites due to the transfer of photo-generated electrons from $LaFeO_3$. Moreover, the ratio of Pd^0 to Pd^{4+} still maintained a high value even with a slight increase when visible light was introduced into the reaction process. According to the *in-situ* DRIFTS results in Figs. 8–10, it was the higher surface electron density of Pd/$LaFeO_3$ to be mainly responsible for the stability of catalytic activity of Pd/$LaFeO_3$ under visible light irradiation.

Based on the above XPS results, it was proposed that: (1) Visible light irradiation could promote the formation of surface oxygen vacancies over $LaFeO_3$ and maintain surface electron density of O and Fe atoms. (2) CO and NO adsorbed on the surface of catalyst samples could directly react with the surface hydroxyl or the surface lattice oxygen to form the carbonate and nitrate active intermediates. (3) The thermal reaction would result in the reduction of Pd^{4+} located at the lattice of $LaFeO_3$, while visible light irradiation further accelerated the process due to the transfer of photo-generated electrons from $LaFeO_3$ to Pd nanoparticles accompanied with enriched surface electron density of Pd^0 sites. (4) The photo-thermal synergistic effect could facilitate the oxygen release/storage process of $LaFeO_3$. The above common effects would promote the adsorption and activation of NO and CO over Pd/$LaFeO_3$, and finally accelerate the oxidation of CO and reduction of NO. This electron transfer behavior between Pd and $LaFeO_3$ could be described in Fig. 12(a) and (b).

Moreover, to further reveal the interface charge transfer behavior between $LaFeO_3$ and Pd, the transient photocurrent responses of the samples were carried out by several on-off cycles of visible light irradiation (≥420 nm). As shown in Fig. 13, $LaFeO_3$ itself (as a semiconductor) exhibited an apparent photocurrent induced by the electron

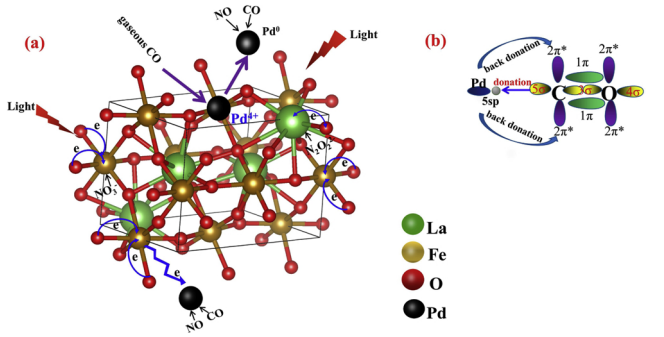

Fig. 12. The possible charge transfer behavior between Pd and $LaFeO_3$ during the process of CO + NO reaction under visible light irradiation. (a) $LaFeO_3$ (from O_{2p} to Fe_{3d} orbit induced by visible light irradiation) donated electrons to adjacent Pd nanoparticles. Additionally, the Pd^{4+} would be reduced by the CO stream then to form metallic Pd nanoparticles; (b) The donation process was that the electrons transferred from the CO 5σ orbits to empty Pd 5sp orbits, and the back-donation process was that the electron enriched 5sp orbits of Pd interacted with the 2π* orbits of CO then weakened the bond of C–O (the interaction between NO and catalyst sample similar to CO).

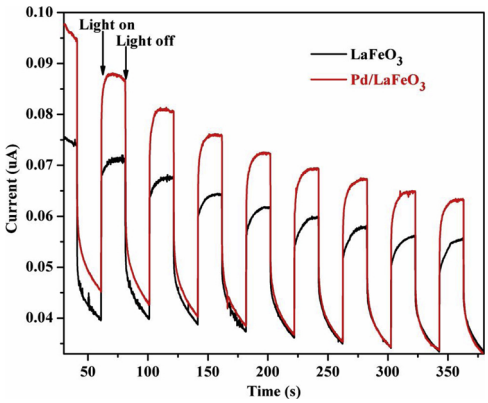

Fig. 13. Transient photocurrent responses of the samples in a 0.1 M Na_2SO_4 aqueous solution under visible light irradiationt (≥420 nm) or not.

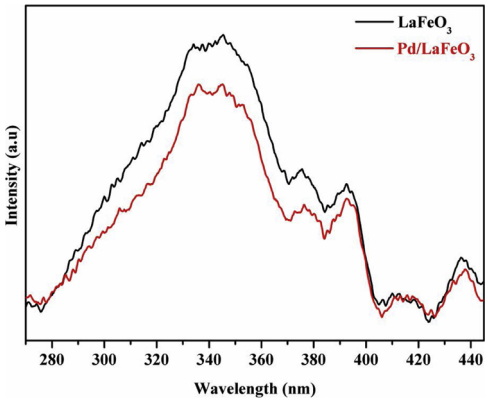

Fig. 14. PL spectra of $LaFeO_3$ and $Pd/LaFeO_3$ samples under excited by 240 nm light.

transfer from O_{2p} to Fe_{3d} under visible light excitation. Note that the photocurrent of $LaFeO_3$ was enhanced significantly by the loading of Pd, which demonstrated the more efficient charge separation and transfer over $Pd/LaFeO_3$ sample under visible light irradiation and also well accounted for the much higher catalytic activity of $Pd/LaFeO_3$ than Pd-free $LaFeO_3$ support toward the reduction of NO in CO stream. Furthermore, the migration and recombination processes of the photo-generated charge carriers could be also confirmed by the Photoluminescence (PL) spectra. As shown in Fig. 14, the stronger photoluminescence quenching for the $Pd/LaFeO_3$ compared to bare $LaFeO_3$ support suggested that the introduction of Pd could effectively suppress the recombination of photo-generated charge carries on $LaFeO_3$, resulting in a longer lifetime of surface electrons on $Pd/LaFeO_3$.

3.5. Proposed mechanism of CO/NO redox reaction over $Pd/LaFeO_3$

Further on the basis of the above mentioned analyses under visible light irradiation or not, we suggested that the adsorption and activation behavior of CO or NO at $Pd/LaFeO_3$ were mainly determined by the surface electron density of Pd and $LaFeO_3$ sites. Moreover, the release/storage oxygen process of $LaFeO_3$ could promote the generation of oxygen vacancies then be favorable for the increase in surface chemisorption oxygen for NO and CO activation, while visible light irradiation could further strengthen the electron transfer from $LaFeO_3$ to Pd sites by exciting $LaFeO_3$.

Referring to the thermo-catalytic process of NO + CO reaction [6–8] and our previous works over the supported Pt catalysts [15], the reaction process of CO + NO over $Pd/LaFeO_3$ under visible light irradiation could be described as follows. The numbers in the equation represented the adsorption sites in the *in-situ* DRIFTS spectra:

(1) Generation and transfer of photo-excitation electrons

- Photo-excitation of $LaFeO_3$:

$$LaFeO_3 + h\nu \rightarrow LaFeO_3 \quad (e_{cb}{}^{-}\text{-}Fe_{3d},\ h_{vb}{}^{+}\text{-}O_{2p})$$

- $LaFeO_3$ went through an oxygen release/storage process by accepting the photo-generated electrons:

$$LaFeO_3 + e_{cb}{}^{-} \leftrightarrow LaFeO_{3-x} + xO_L{}^{2-} \quad \text{(release oxygen process)}$$

- Photo-generated electrons transfer from $LaFeO_3$ to Pd sites:

$$Pd + e_{cb}{}^{-} \rightarrow Pd(e)$$

- Adsorption processes of CO and NO
  - ○ CO and NO were adsorbed at electron-rich Pd sites:

$$Pd(e) + CO \rightarrow \{Pt\text{–}C\equiv O\}\ (2080\ cm^{-1})$$

$$Pd(e) + NO \rightarrow \{Pd\text{–}NO\}\ (1750\ cm^{-1})$$

- NO was adsorbed at La^{3+} sites (due to the existence of SOV induced by the $LaFeO_3$ releasing oxygen process) in the state of cis-$N_2O_2{}^{2-}$:

$$2La^{3+}\text{-}[SOV] + 2NO \rightarrow 2La^{3+}\text{-}N_2O_2{}^{*}\ (1090\ cm^{-1})$$

- NO was adsorbed at Fe sites or SOV and then reacted with lattice oxygen to form bridging bidentate nitrate species:

$$NO + Fe^{3+}\text{-}[SOV] \rightarrow Fe^{3+}\text{-}NO\ (1810\ cm^{-1})$$

$$Fe^{3+}\text{-}NO + LaFeO_3\ (O_L) \rightarrow Fe^{3+}\text{-}NO_3{}^{*}\ (1620\ cm^{-1})$$

- Adsorbed NO species reacting with CO species by four pathways
  - ○ Pathway I: $N_2O_2{}^{2-}$ species formed at La sites preferentially react with CO adsorbed at Pd sites to produce N_2 and CO_2 due to its lower oxidation state:

$$La^{3+}\text{-}N_2O_2{}^{*} + \{Pd\text{–}C\equiv O\} \rightarrow CO_2 + N_2 + Pd + La^{3+}$$

  - ○ Pathway II: Formed unidentate nitrate species at La sites reacted with the activated CO adsorbed at Pd sites to form higher

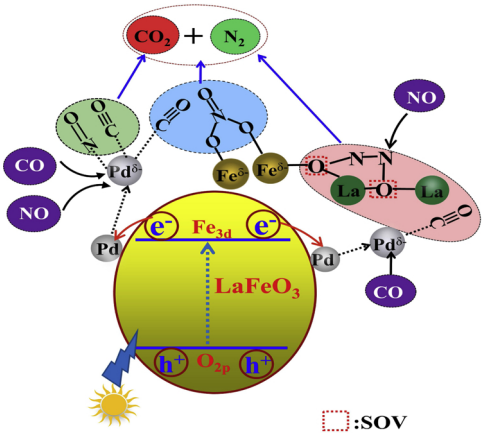

Fig. 15. The proposed process of CO + NO redox reaction over Pd/$LaFeO_3$ under visible light irradiation.

oxidized carbonate and lower oxidized monodentate nitrites, and then produced N_2 and CO_2 (a main pathway)

$$La\text{-}NO_3^* \ (1522\ cm^{-1}) + Pd\text{-}COO^* \ (1516\ cm^{-1}) \rightarrow La\text{-}NO_2^* \ (1434\ cm^{-1}) + Pd\text{-}CO_3^* \ (1665\ cm^{-1})$$

$$La\text{-}NO_2^* + \{Pd\text{–}C\equiv O\} \rightarrow CO_2 + N_2 + Pd + La^{3+}$$

$$Pd\text{-}CO_3^* \xrightarrow{\text{decomposation}} CO_2 + Pd$$

○ Pathway III: Formed bridging bidentate nitrate species at Fe sites reacted with the activated CO adsorbed at Pd sites to form –NCO or N_2O species, and then produce N_2 and CO_2:

$$Fe^{n+}\text{-}NO_3^* + \{Pd\text{–}C\equiv O\} \rightarrow NCO^* \ (2204\ cm^{-1}) + N_2O + Fe^{n+} + Pd$$

$$2Pd\text{-}NCO \rightarrow N_2 + CO_2 + 2Pd$$

$$N_2O + Fe^{3+}\text{-}[SOV] \rightarrow N_2 + Fe^{4+}\text{-}[O_L]$$

○ Pathway IV: NO species adsorbed at Pd sites react with CO adsorbed at Pd sites to form Pd-NCO or N_2O species, and then produce N_2 and CO_2:

$$\{Pd\text{-}NO\} + \{Pd\text{–}C\equiv O\} \rightarrow Pd\text{–}N{=}C{=}O \ (2204\ cm^{-1}) + N_2O \ (2240\ cm^{-1})$$

$$2Pd\text{-}NCO \rightarrow N_2 + CO_2 \ (2358\ cm^{-1}) + 2Pd$$

$$\{Pd\text{–}CO\} + \{Pd\text{–}N{=}N{=}O\} \rightarrow N_2 + CO_2 + 2Pd$$

- The produced electrons will recombine with holes

$$LaFeO_3\ (e_{cb}) + LaFeO_3\ (h_{vb}) \rightarrow LaFeO_3$$

The above proposed mechanism of CO reaction with NO over Pd/$LaFeO_3$ under visible light irradiation could also be described in Fig. 15.

During the above processes, the adsorption and activation of NO at Fe and La sites may be the key steps, and then the formed intermediates would be further reacted via different pathways (main Pathways I–III). Under visible light irradiation, the photo-generated electrons induced by $LaFeO_3$ could transfer to Pd, resulting in the increase in surface electron density of Pd sites. Meanwhile, $LaFeO_3$ itself acted as an active site to take part in the reaction process. More importantly, the reducibility of $LaFeO_3$ induced by visible light (Fe^{4+}/Fe^{3+}, i.e., the release/storage oxygen behavior of $LaFeO_{3-x}$) would be beneficial to maintain the higher stability of catalytic activity. This study implies that the photo-excitation behavior of support maybe acts as an electron additive to promote thermal catalytic reaction of NO + CO.

4. Conclusions

In this work, the Pd/$LaFeO_3$ samples were prepared by a two-step co-precipitation method and deposition-precipitation methods. After evaluating its catalytic performance of redox CO + NO under visible light or not and combining with the above characterization results, the following conclusions could be drawn:

(I) Compared to the sole $LaFeO_3$, Pd/$LaFeO_3$ exhibited higher catalytic activity and selectivity of N_2 for CO + NO reaction either reaction under visible light irradiation or in dark.

(II) Based on the results of DRS, XPS, TPD – Mass and *in-situ* DRIFTS, it was proposed that this promotional effects of visible light in reduction of NO by CO to N_2 could be mainly attributed to the photo-excited electron transfer from $LaFeO_3$ support to the loaded Pd nanoparticles, resulting in the enrichment of surface electron density of Pd and the subsequent enhanced adsorption and activation of CO and NO molecules at Pd sites.

(III) Visible light could further promote the generation of the surface oxygen vacancies over $LaFeO_3$ support, resulting in the sustained release/storage oxygen (Fe^{4+}/Fe^{3+}) process then keeping a higher stability of catalytic activity over Pd/$LaFeO_3$ than in dark. This study shows that the photo-excitation behavior of $LaFeO_3$ support maybe acted as an electron additive to be introduced into a thermal catalytic reaction of NO + CO over the metal supported catalyst.

Acknowledgments

This work was financially supported by the National Natural Science Foundation of China (nos. 21872030 and 21272037), the National Basic Research Program of China (973 Program, no. 2014CB239303) and the Science & Technology Plan Project of Fujian Province (no. 2014Y2003).

Appendix A. Supplementary data

Supplementary data associated with this article can be found, in the online version, at https://doi.org/10.1016/j.apcatb.2019.03.029.

References

[1] S. Roy, M.S. Hegde, G. Madras, Catalysis for NO_x abatement, Appl. Energy 86 (2009) 2283–2297.
[2] P. Granger, J.J. Lecomte, L. Leclercq, G. Leclercq, An attempt at modelling the activity of Pt–Rh/Al_2O_3 three-way catalysts in the CO + NO reaction, Appl. Catal. A: Gen. 208 (2001) 369–379.
[3] P. Granger, F. Dhainaut, S. Pietrzik, P. Malfoy, A.S. Mamede, L. Leclercq, G. Leclercq, An overview: comparative kinetic behaviour of Pt, Rh and Pd in the NO + CO and NO + H_2 reactions, Top. Catal. 39 (2006) 65–76.
[4] M. Uenishi, H. Tanaka, M. Taniguchi, I. Tan, Y. Sakamoto, S.-i. Matsunaga, K. Yokota, T. Kobayashi, The reducing capability of palladium segregated from perovskite-type $LaFePdO_x$ automotive catalysts, Appl. Catal. A: Gen. 296 (2005) 114–119.
[5] A. Glisenti, M. Pacella, M. Guiotto, M.M. Natile, P. Canu, Largely Cu-doped $LaCo_{1-x}Cu_xO_3$ perovskites for TWC: toward new PGM-free catalysts, Appl. Catal. B: Environ. 180 (2016) 94–105.
[6] X. Yao, Y. Xiong, W. Zou, L. Zhang, S. Wu, X. Dong, F. Gao, Y. Deng, C. Tang, Z. Chen, L. Dong, Y. Chen, Correlation between the physicochemical properties and catalytic performances of $Ce_xSn_{1-x}O_2$ mixed oxides for NO reduction by CO, Appl. Catal. B: Environ. 144 (2014) 152–165.
[7] L. Wang, X. Cheng, Z. Wang, C. Ma, Y. Qin, Investigation on Fe–Co binary metal oxides supported on activated semi-coke for NO reduction by CO, Appl. Catal. B: Environ. 201 (2017) 636–651.
[8] Y. Lv, L. Liu, H. Zhang, X. Yao, F. Gao, K. Yao, L. Dong, Y. Chen, Investigation of surface synergetic oxygen vacancy in CuO–CoO binary metal oxides supported on gamma-Al_2O_3 for NO removal by CO, J. Colloid Interface Sci. 390 (2013) 158–169.
[9] A. Linsebigler, G. Lu, J.T. Yates, CO chemisorption on TiO_2(110): oxygen vacancy site influence on CO adsorption, J. Chem. Phys. 103 (1995) 9438–9443.

[10] W. Dai, X. Chen, X. Zheng, Z. Ding, X. Wang, P. Liu, X. Fu, Photocatalytic oxidation of CO on TiO_2: chemisorption of O_2, CO, and H_2, ChemPhysChem 10 (2009) 411–419.

[11] Z.M. El-Bahy, Adsorption of CO and NO on ceria- and Pt-supported TiO_2: in situ FTIR study, Mod. Res. Catal. 2 (2013) 136–147.

[12] K. Yang, J. Liu, R. Si, X. Chen, W. Dai, X. Fu, Comparative study of Au/TiO_2 and Au/Al_2O_3 for oxidizing CO in the presence of H_2 under visible light irradiation, J. Catal. 317 (2014) 229–239.

[13] L. Lin, K. Wang, K. Yang, X. Chen, X. Fu, W. Dai, The visible-light-assisted thermocatalytic methanation of CO_2 over Ru/$TiO_{(2-x)}N_x$, Appl. Catal. B: Environ. 204 (2017) 440–455.

[14] X. Lin, L. Lin, K. Huang, X. Chen, W. Dai, X. Fu, CO methanation promoted by UV irradiation over Ni/TiO_2, Appl. Catal. B: Environ. 168–169 (2015) 416–422.

[15] K. Huang, L. Lin, K. Yang, W. Dai, X. Chen, X. Fu, Promotion effect of ultraviolet light on NO + CO reaction over Pt/TiO_2 and Pt/CeO_2–TiO_2 catalysts, Appl. Catal. B: Environ. 179 (2015) 395–406.

[16] X.P. Dai, J. Li, J.T. Fan, W.S. Wei, J. Xu, Synthesis gas generation by chemical-looping reforming in a circulating fluidized bed reactor using perovskite $LaFeO_3$-based oxygen carriers, Ind. Eng. Chem. Res. 51 (2012) 11072–11082.

[17] Y. Zheng, K. Li, H. Wang, D. Tian, Y. Wang, X. Zhu, Y. Wei, M. Zheng, Y. Luo, Designed oxygen carriers from macroporous $LaFeO_3$ supported CeO_2 for chemical-looping reforming of methane, Appl. Catal. B: Environ. 202 (2017) 51–63.

[18] Q. Peng, B. Shan, Y. Wen, R. Chen, Enhanced charge transport of $LaFeO_3$ via transition metal (Mn, Co, Cu) doping for visible light photoelectrochemical water oxidation, Int. J. Hydrogen Energy 40 (2015) 15423–15431.

[19] Z.X. Li, F.B. Shi, C.H. Yan, Controllable assembly of hierarchical macro-porous–mesoporous $LnFeO_3$ and their catalytic performance in the CO + NO reaction, Langmuir 31 (2015) 8672–8679.

[20] K. Zhou, H. Chen, Q. Tian, Z.P. Hao, D.X. Shen, X.B. Xu, Pd-containing perovskite-type oxides used for three-way catalysts, J. Mol. Catal. A: Chem. 189 (2002) 225–232.

[21] Y. Nishihata, J. Mizuki, T. Akao, et al., Self-regeneration of a Pd-perovskite catalyst for automotive emissions control, Nature 418 (6894) (2002) 164.

[22] S. Thirumalairajan, K. Girija, V.R. Mastelaro, N. Ponpandian, Photocatalytic degradation of organic dyes under visible light irradiation by floral-like $LaFeO_3$ nanostructures comprised of nanosheet petals, New J. Chem. 38 (2014) 5480–5490.

[23] J. Li, W. Guan, X. Yan, Z. Wu, W. Shi, Photocatalytic ozonation of 2,4-dichlorophenoxyacetic acid using $LaFeO_3$ photocatalyst under visible light irradiation, Catal. Lett. 148 (2017) 23–29.

[24] H. Abdulhamid, J. Dawody, E. Fridell, M. Skoglundh, A combined transient in situ FTIR and flow reactor study of NO_x storage and reduction over M/$BaCO_3$/Al_2O_3 (M = Pt, Pd or Rh) catalysts, J. Catal. 244 (2006) 169–182.

[25] M. Valden, R.L. Keiski, N. Xiang, J. Pere, J. Aaltonen, M. Pessa, T. Maunula, A. Savimäki, A. Lahti, M. Härkönen, Reactivity of Pd/Al_2O_3, Pd/La_2O_3–Al_2O_3 and Pd/$LaAlO_3$ catalysts for the reduction of NO by CO: CO and NO adsorption, J. Catal. 161 (1996) 614–625.

[26] E. Ozensoy, D. Wayne Goodman, Vibrational spectroscopic studies on CO adsorption, NO adsorption CO + NO reaction on Pd model catalysts, Phys. Chem. Chem. Phys. 6 (2004) 3765.

[27] A. Ueda, T. Nakao, M. Azuma, T. Kobayashi, Two conversion maxima at 373 and 573 K in the reduction of nitrogen monoxide with hydrogen over Pd/TiO_2 catalyst, Catal. Today 45 (1998) 135.

[28] M. Popa, J. Frantti, M. Kakihana, Lanthanum ferrite $LaFeO_{3+\delta}$ nanopowders obtained by the polymerizable complex method, Solid State Ion. 154–155 (2002) 437–445.

[29] M. Romero, R.W. Gómez, V. Marquina, J.L. Pérez-Mazariego, R. Escamilla, Synthesis by molten salt method of the $AFeO_3$ system (A = La, Gd) and its structural, vibrational and internal hyperfine magnetic field characterization, Physica B: Condens. Matter 443 (2014) 90–94.

[30] D. Blanck, A. Schön, A.-S. Mamede, C. Dujardin, J.-P. Dacquin, P. Granger, J.-F. Paul, E. Berrier, *In situ* Raman spectroscopy evidence of an accessible phase potentially involved in the enhanced activity of La-deficient lanthanum orthoferrite in 3-way catalysis (TWC), Catal. Today 283 (2017) 151–157.

[31] W.-Y. Lee, H.J. Yun, J.-W. Yoon, Characterization and magnetic properties of $LaFeO_3$ nanofibers synthesized by electrospinning, J. Alloys Compd. 583 (2014) 320–324.

[32] S.B. Varandili, A. Babaei, A. Ataie, Characterization of B site codoped LaFeO3 nanoparticles prepared via co-precipitation route, Rare Metals. 37 (2016) 181–190.

[33] D.Y. Yoon, Y.J. Kim, J.H. Lim, B.K. Cho, S.B. Hong, I.-S. Nam, J.W. Choung, Thermal stability of Pd-containing LaAlO3 perovskite as a modern TWC, J. Catal. 330 (2015) 71–83.

[34] S.K. Mohapatra, N. Kondamudi, S. Banerjee, M. Misra, Functionalization of self-organized TiO_2 nanotubes with Pd nanoparticles for photocatalytic decomposition of dyes under solar light illumination, Langmuir 24 (2008) 11276–11281.

[35] S. Zhao, Y. Wang, L. Wang, Y. Jin, Preparation, characterization and catalytic application of hierarchically porous $LaFeO_3$ from a pomelo peel template, Inorg. Chem. Front. 4 (2017) 994–1002.

[36] Y. Feng, G. Wang, J. Liao, W. Li, C. Chen, M. Li, Z. Li, Honeycomb-like ZnO mesoporous nanowall arrays modified with Ag nanoparticles for highly efficient photocatalytic activity, Sci. Rep. 7 (2017) 11622.

[37] Y. Zhang, Q. Li, C. Liu, X. Shan, X. Chen, W. Dai, X. Fu, The promoted effect of a metal-organic frameworks (ZIF-8) on Au/TiO_2 for CO oxidation at room temperature both in dark and under visible light irradiation, Appl. Catal. B: Environ. 224 (2018) 283–294.

[38] L. Qi, Q. Yu, Y. Dai, C. Tang, L. Liu, H. Zhang, F. Gao, L. Dong, Y. Chen, Influence of cerium precursors on the structure and reducibility of mesoporous CuO–CeO_2 catalysts for CO oxidation, Appl. Catal. B: Environ. 119–120 (2012) 308–320.

[39] L.F. Liao, C.F. Lien, D.L. Shieh, M.T. Chen, J.L. Lin, FTIR study of adsorption and photoassisted oxygen isotopic exchange of carbon monoxide, carbon dioxide, carbonate, and formate on TiO_2, J. Phys. Chem. B 106 (2002) 11240–11245.

[40] J.-W. Lee, X.L. Piao, Y.-K. Yun, J.-I. Jin, Y.-S. Kang, W.-C. Zin, Synthesis and liquid crystalline properties of T-shaped dimesogenic compound, Liq. Cryst. 26 (1999) 1671–1685.

[41] M. Wongaree, S. Chiarakorn, S. Chuangchote, Photocatalytic improvement under visible light in TiO_2 nanoparticles by carbon nanotube incorporation, J. Nanomater. 2015 (2015) 1–10.

[42] N. Weiher, A.M. Beesley, N. Tsapatsaris, L. Delannoy, C. Louis, J.A. Van Bokhoven, S.L.M. Schroeder, Activation of oxygen by metallic gold in Au/TiO_2 catalysts, J. Am. Chem. Soc. 129 (2007) 2240–2241.

[43] J. Sá, J.A. Anderson, FTIR study of aqueous nitrate reduction over Pd/TiO_2, Appl. Catal. B: Environ. 77 (2008) 409–417.

[44] L. Liu, Y. Chen, L. Dong, J. Zhu, H. Wan, B. Liu, B. Zhao, H. Zhu, K. Sun, L. Dong, Y. Chen, Investigation of the NO removal by CO on CuO–CoO_x binary metal oxides supported on $Ce_{0.67}Zr_{0.33}O_2$, Appl. Catal. B: Environ. 90 (2009) 105–114.

[45] L.J. Lobree, I.C. Hwang, J.A. Reimer, A.T. Bell, An *in situ* infrared study of NO reduction by C_3H_8 over Fe-ZSM-5, Catal. Lett. 63 (1999) 233–240.

[46] B. Klingenberg, M.A. Vannice, NO adsorption and decomposition on La_2O_3 studied by DRIFTS, Appl. Catal. B: Environ. 21 (1999) 19–33.

[47] W. Yang, R. Zhang, B. Chen, D. Duprez, S. Roye, New aspects on the mechanism of C_3H_6 selective catalytic reduction of NO in the presence of O_2 over $LaFe_{1-x}$(Cu, Pd)$_xO_{3-\delta}$ perovskites, Environ. Sci. Technol. 46 (2012) 11280–11288.

[48] E. Guglielminotti, F. Boccuzzi, Study of the NO, reaction with reducing gases on Fe/ZrO_2, catalyst, Appl. Catal. B: Environ. 8 (1996) 375–390.

[49] W. Weisweiler, K. Hizbullah, S. Kureti, Simultaneous catalytic conversion of NO_x and soot from diesel engines exhaust into nitrogen and carbon dioxide, Chem. Eng. Technol. 25 (2002) 140–143.

[50] R. Dudric, A. Vladescu, V. Rednic, M. Neumann, I.G. Deac, R. Tetean, XPS study on $La_{0.67}Ca_{0.33}Mn_{1-x}Co_xO_3$ compounds, J. Mol. Struct. 1073 (2014) 66–70.

[51] D.J. Lam, B.W. Veal, D.E. Ellis, Electronic structure of lanthanum perovskites with 3d transition elements, Phys. Rev. B 22 (1980) 5730–5739.

[52] W. Göpel, J.A. Anderson, D. Frankel, M. Jaehnig, K. Phillips, J.A. Schafer, G. Rocker, Surface defects of TiO_2 (110): a combined XPS, XAES and ELS study, Surf. Sci. 139 (1984) 333–346.

[53] E. Cao, T. Cui, Y. Yang, Y. Zhang, W. Hao, L. Sun, H. Peng, Simultaneous control of electrical and magnetic properties of $LaFeO_{3-\delta}$ nanoparticles by contact of ethanol gas, Mater. Lett. 190 (2017) 143–145.

[54] J.M. Giraudon, A. Elhachimi, G. Leclercq, Catalytic oxidation of chlorobenzene over Pd/perovskites, Appl. Catal. B: Environ. 84 (2008) 251–261.

[55] M. Uenishi, M. Taniguchi, H. Tanaka, M. Kimura, Y. Nishihata, J. Mizuki, T. Kobayashi, Redox behavior of palladium at start-up in the perovskite-type $LaFePdO_x$ automotive catalysts showing a self-regenerative function, Appl. Catal. B: Environ. 57 (2005) 267–273.